ACS Energy LETTERS

http://pubs.acs.org/journal/aelccp
Letter

The Physics of Ultra-Long Cooling Times in Metal Halide Perovskites

Published as part of ACS Energy Letters special issue "The Evolving Landscape of Energy Research: Insights from Leading Researchers".

Tim Faber, Larissa J. M. van de Ven, Lado Filipovic, Maria Antonietta Loi, and L. Jan Anton Koster*

Cite This: https://doi.org/10.1021/acsenergylett.6c00547

ABSTRACT: Ultra-long cooling times are the most crucial ingredient for the successful development of a hot-carrier solar cell. Recent experimental reports for metal halide perovskites show the possibility of reaching these relevant values using Sn-based perovskite compositions, due to their low effective mass. In this work, the governing underlying physics is uncovered by investigating the interplay between band filling and the hot phonon bottleneck effect. By using ensemble Monte Carlo simulations and through comparison with time-resolved photoluminescence measurements, it is demonstrated that solely the combination of these two phenomena is sufficient to reproduce ultra-long carrier cooling times. The dependency of band filling on material parameters is analyzed, and it is crucially shown that carriers affected by band filling remain hot in terms of their Fermi–Dirac temperature for the remainder of their energy relaxation period. Our results are important in the discussion regarding the suitability of metal halide perovskites for future HCSC applications, and function as a road-map towards the successful construction of a perovskite-based HCSC.

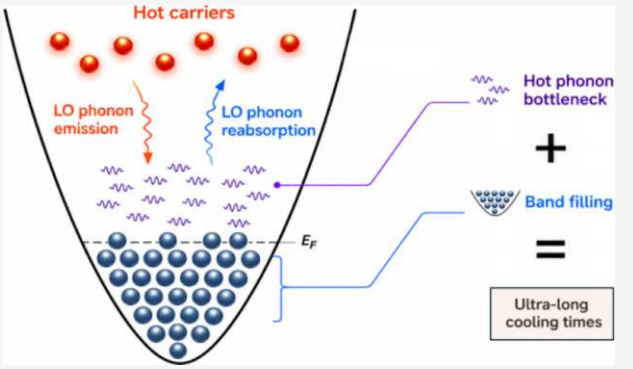

The aim of a hot carrier solar cell (HCSC) is to break the Shockley–Queisser limit by harvesting photo-excited carriers before they have lost their surplus of thermal energy.[1,2] The crucial feature a HCSC material should possess is a very long carrier cooling time.[3,4] Carrier cooling or relaxation times should be on the order of radiative recombination times, which comes down to nanosecond timescales.[5,6]

Nanosecond relaxation times are highly unusual, as carriers typically cool down within a picosecond.[7] Promisingly, several recent experimental studies regarding Sn-based metal halide perovskites (MHP), have reported cooling times up to several nanoseconds.[8,9]

Carrier cooling times in MHPs show significant variation for different chemical compositions.[10−12] A range of physical phenomena has already been put forward in an attempt to explain the underlying photophysics.[13−21] To explain the ultra-long cooling times, a combination of two physical phenomena, band filling and the hot phonon bottleneck (HPB), was suggested by the authors.[8,18]

Photoinduced band filling is also known as the dynamic Burstein–Moss (BM) effect.[22,23] The BM effect is shown in Figure 1 and characterized by a BM shift: An apparent blueshifting of the peak energy in the photoluminescence spectra. A BM shift is the result of the occupation of lower-energy states by previously photo-excited carriers that have relaxed back down after LO phonon emission.[24,25] Enhanced band filling is expected for Sn-based perovskites due to the very narrow electronic density of states at the valence band edge.[18,26]

Additionally, the HPB effect was shown to play a central role, especially for organic–inorganic perovskites.[16,27] Due to shorter dephasing times of the relevant phonon modes, caused by increased anharmonicity due to additional rotational degrees of freedom of the organic cation, the formamidinium (FA) or methylammonium (MA) based perovskite systems exhibit stronger phononic coupling, resulting in higher phonon upconversion probabilities and therefore an amplified HPB effect.[18,28]

In a recent paper,[27] we have shown that the HPB effect can lead to cooling times that are significantly longer than the phonon lifetime. At low carrier densities, the cooling time is predominantly set by the phonon lifetime. However, carriers also reabsorb phonons, and the reabsorption rate increases with the phonon concentration. At high carrier densities, the phonon occupation number increases, and reabsorption of phonons by carriers outcompetes phonon decay. As a result, charge carriers can remain hot as any phonon emission is quickly compensated for by phonon reabsorption.[27]

Received: February 20, 2026
Revised: July 15, 2026
Accepted: July 24, 2026

https://doi.org/10.1021/acsenergylett.6c00547
ACS Energy Lett. XXXX, XXX, XXX−XXX

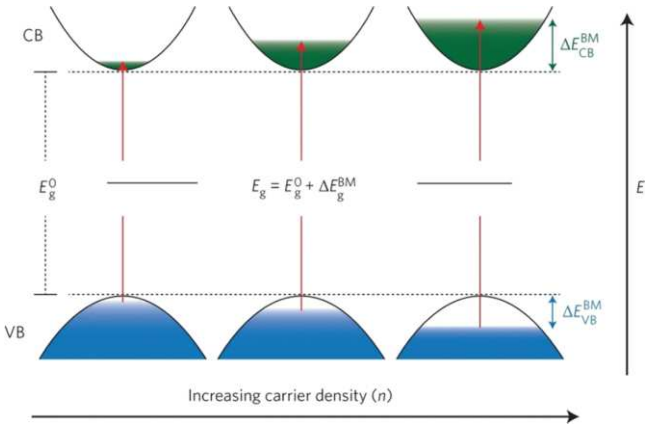

Figure 1. The Burstein–Moss (BM) effect. Lower lying energy states are being filled by photo-excited carriers that are cooling down, resulting in an apparent increase of the bandgap energy by ΔE_{BM}. Image adapted from ref 25.

While the ability of the HPB effect to extend cooling by orders of magnitude has been established,[16,27,29–31] the potential of band filling is unclear. Furthermore, the question whether carriers are still 'hot' in terms of the Fermi–Dirac temperature is still an open question.[18] Understanding the synergy of band filling and the HPB effect is crucial in fully capturing the potential of these effects to extend cooling times to the nanosecond range.

In this work, an investigation of the interplay between band filling and the HPB effect is presented. Remarkably, it is demonstrated that a combination of these two phenomena alone is able to produce ultra-long carrier cooling times. Crucially, we establish that carriers remain at an elevated FD temperature for the entirety of the cooling process.

Our findings show the desired ultra-long cooling times specifically for tin-based perovskite systems, indicating its strong potential for future HCSC applications. These results are important in unraveling the underlying physics of slow hot carrier cooling in MHPs and the discussion regarding the suitability of metal halide perovskites for HCSC applications. With this work, we present a roadmap towards the successful construction of a perovskite-based HCSC.

The investigation is executed by performing hot carrier simulations using an ensemble Monte Carlo framework.[32–36] The EMC is a proven methodology for handling nonequilibrium charge transport problems,[37] and is the perfect vehicle to investigate the interaction dynamics of multiple physical phenomena. For further details on the EMC method, we direct the reader to the Methods section in the Supporting Information and our previous papers.[12,27]

The model describes the carrier-LO phonon interactions via the Fröhlich interaction under a single-mode approximation. Although an accurate description of certain transport observables, such as the temperature dependence of the mobility, requires several phonon branches to be retained,[38,39] the attendant complexity can be sidestepped by folding the branches into one effective mode.[40–43] Such an effective mode blends the contributions of the individual branches and oscillates at a single representative frequency.

For the following simulations, we have turned off the HPB effect to focus solely on the dynamics of band filling.

A BM shift can be expressed in terms of the effective mass and carrier density (Figure 1):[44]

$$\Delta E_g^{BM} = \frac{h^2}{2\mu}(3\pi^2 n)^{2/3} \tag{1}$$

where μ is the reduced effective mass given by $\mu^{-1} = m_e^{-1} + m_h^{-1}$, and n the carrier density.

A BM shift characterizes a degenerate semiconductor, showing adherence to Fermi–Dirac (FD) statistics. The Pauli exclusion principle forces electrons to consecutive higher-lying energy states. Particles are distributed according to the FD distribution function, given by

$$f(E) = \frac{1}{e^{(E-\mu)/k_B T} + 1} \tag{2}$$

The classical Maxwell–Boltzmann distribution, characterized by the exponential function $\exp(-E/k_B T)$, no longer holds when quantum effects become non-negligible, as is the case at sufficiently low temperatures, or in our case, sufficiently high chemical potential.

The temperature of a FD system is inversely proportional to the magnitude of the slope of the FD function evaluated at the Fermi level via:

$$\left.\frac{df}{dE}\right|_{E_F} = -\frac{1}{4_{kB} T} \tag{3}$$

and illustrated in Figure 2.

The second parameter of the FD model, the chemical potential μ, is defined as the energy at which the FD distribution function equals one-half, $f(E) = \frac{1}{2}$, for any temperature. It is better understood as the energy at which a state has a 50% probability of being occupied. It is a measure of how many of the available states are filled, and is therefore directly related to the BM-shift. It equals the Fermi energy at $T = 0$, and will be marginally lower at finite T due to the effect of the temperature on the distribution.[45]

All of them are connected via the carrier density given by

$$n = \int_{E\min}^{\infty} g(E) \frac{1}{e^{(E-\mu)/k_B T} + 1} dE \tag{4}$$

with $g(E)$ the density of states. When solving the above equation for the chemical potential μ at $T = 0$, one ends up with the expression for the BM shift, eq 1, recognized as the Fermi energy.

In our simulations, the FD temperature and chemical potential are obtained by fitting the energy distribution to a FD distribution, yielding a value for both.

A stronger BM shift can be expected for a smaller effective mass and at larger particle density. Equation 1 is recognized as the Fermi energy at 0 K.[45] Here, a parabolic band dispersion is assumed.

In Figure 3, the effects of the different parameters influencing band filling are presented. The effects of the carrier density ρ, Figure 3a, and the effective mass m*, Figure 3b, are presented. Here, a perovskite-like system is used with $m^* = 0.2$, $\varepsilon_0 = 30$, $\varepsilon_\infty = 8$, and $\omega_0 = 31$ ps^{-1}, comparable to a Pb-based perovskite with a lighter halide such as bromide.[12] In Figure 3a, at a higher particle density, the lower energy states quickly fill up and inhibit the further decrease of kinetic energy from other carriers.

https://doi.org/10.1021/acsenergylett.6c00547
ACS Energy Lett. XXXX, XXX, XXX–XXX

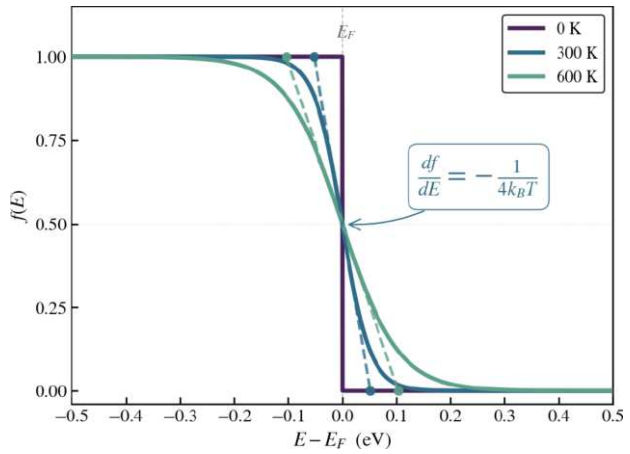

Figure 2. The FD distribution for different temperatures 0, 300 and 600 K. In the FD regime, the temperature is evaluated by taking the derivative at the Fermi-level, and is no longer equivalent to the average particle energy.

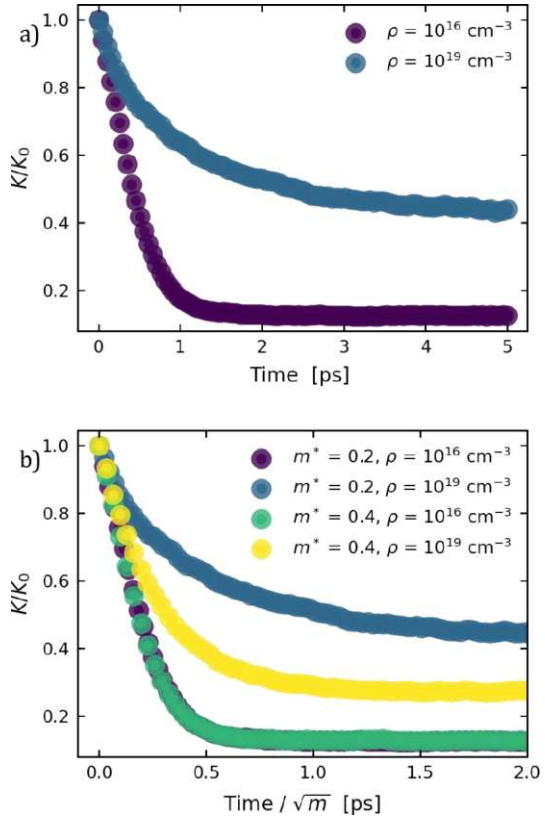

Figure 3. Effect of the carrier density (a) and effective mass (b) on band filling. Here, K/K_0 is the normalized kinetic energy. The system relaxes to a higher average kinetic energy at high density and smaller effective mass. For the effective mass, the time is divided by the square root of the effective mass to obtain overlap at low density, which is not the case at high density as an effect of band filling.

In Figure 3b, the normalized kinetic energy is plotted against the time over the effective mass. This way, we filter out the dependence of the Fröhlich interaction on the effective mass. At low carrier density, cooling happens on the same timescale for both effective masses, as no band filling is occurring. At high carrier density, enhanced band filling is observed for the system with the smaller effective mass. The elevated average kinetic energy is a result of a larger BM shift due to a smaller effective mass (see eq 1).

It is crucial to find out whether or not carriers affected by band filling remain hot in terms of their FD temperature. In Figure 4, a comparison between the behavior of the kinetic energy, chemical potential, and FD temperature is presented for a perovskite-like system of different carrier densities throughout 200 ps. Here a smaller effective mass of $m^* = 0.1$,[46] and smaller phonon frequency of $\omega_0 = 6$ ps^{-1} is used, making the system comparable to tin-based perovskites. Also in these simulations the HPB is turned off.

During the initial 10 ps shown in Figure 4b,c, the system has not yet reached quasiequilibrium; consequently, a FD temperature cannot be accurately assigned. Hence, the assignment of a temperature is not physical. We did not include carrier–carrier interactions in the simulations of Figure 4. Even though it has been shown that at these densities carrier–carrier interactions are relevant,[12,47] they do not play a role in the cooling dynamics. Incorporation of the Coulomb interaction in the Pauli exclusion principle would complicate the simulation unnecessarily.

The behavior of the average kinetic energy in Figure 4a is very similar to what was presented in Figure 3; the average particle energy becomes elevated for a degenerate system. Similarly, Figure 4b shows a similar shift for the chemical potential μ, as the Fermi level shifts up and into the band.

Via the Sommerfeld expansion, one can find that, for a degenerate Fermi system, the average kinetic energy approaches the Fermi-level:[45]

$$<E_{kin}> \Rightarrow \frac{3}{5}\varepsilon_F \tag{5}$$

Substituting the values for the kinetic energy (~0.16 eV) and the chemical potential (~0.24 eV) for the highest carrier density ($\rho = 5 \times 10^{18}$ cm^{-3}) confirms that the system is indeed approaching this limit.

The FD temperature in Figure 4c continues to reach 300 K, even though the average particle energy was observed to shift upward. We can clearly see that the classical Maxwell–Boltzmann approximation, and $E_{kin} = \frac{3}{2}k_BT_{MB}$ no longer holds. As the carrier density increases, the FD temperature cooling time gets extended. This is dramatically visible at $\rho = 5 \times 10^{18}$ cm^{-3}. Even after 200 ps, the FD temperature is still above 600 K.

These results show that indeed an energy shift induced by band filling cannot directly be translated into an increase in temperature. An energy shift for a degenerate system, where FD statistics play a role, is related to a shift in the FD temperature, together with a shift in the chemical potential or Fermi level.[45,48] The Maxwell–Boltzmann temperature approximation is only valid in nondegenerate, classical systems,[49] which is obviously not the case in systems where a BM shift occurs.

The importance of differentiating between the FD temperature, MB temperature, and the average kinetic energy can further be understood when examining the theory behind hot carrier solar cells. A hot carrier solar cell harvests carriers at an elevated FD temperature $T_{e/h}$ above the lattice temperature T_L.[2] In Figure 5, the architecture of a hot carrier solar cell is presented. From Figure 5, we see that the open-circuit voltage V_{OC}

https://doi.org/10.1021/acsenergylett.6c00547
ACS Energy Lett. XXXX, XXX, XXX–XXX

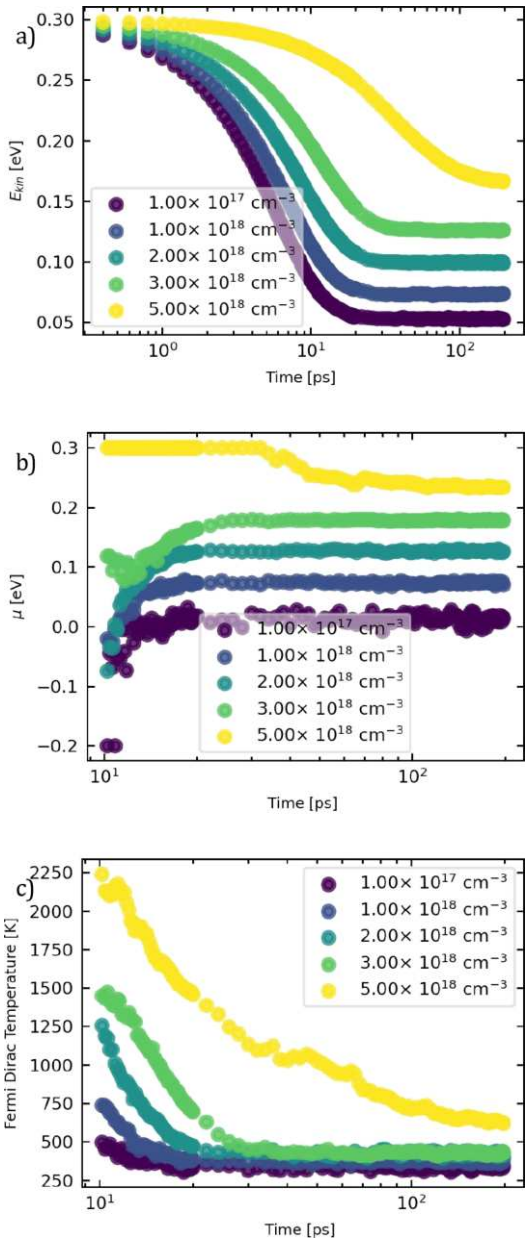

Figure 4. (a) Average kinetic energy, (b) chemical potential, and (c) Fermi–Dirac temperature for a tin perovskite-like system at different densities. For increasing densities, cooling times are extended as energy transfer is limited due to band filling. The FD temperature continues to reach 300 K, while the average kinetic energy is shifting upwards together with the chemical potential, indicating a transition towards the degenerate FD regime.

is proportional to the energy difference ΔE_{eh} between the energy-selective contacts. However, not deducible from the figure is the essential dependence on the carrier FD temperature T_{eh} of the electron and hole distributions:[50]

$$qV_{OC} = \Delta\mu_{eh}\frac{T_L}{T_{eh}} + \Delta E_{eh}\left(1-\frac{T_L}{T_{eh}}\right), \quad (6)$$

where $\Delta\mu_{eh}$ is the difference in quasi Fermi levels $\Delta\mu_{eh} = \mu_e - \mu_h$. The expression assumes $T_e = T_h = T_{eh}$ and reduces to

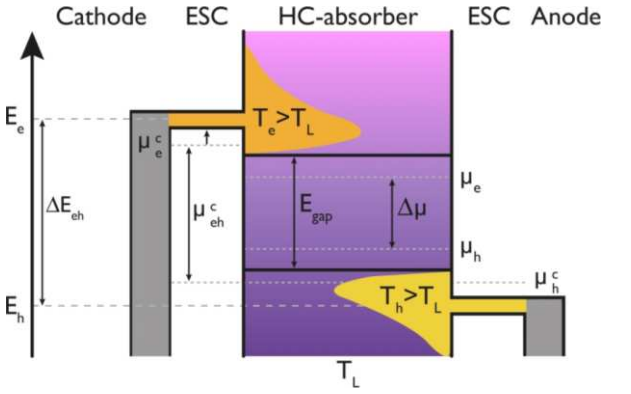

Figure 5. Architecture of a hot carrier solar cell. The absorber layer, characterized by a temperature $T_{e/h}$, is sandwiched between two energy-selective contacts that transport carriers towards the contacts, which remain at T_L. Here $\mu_{e/h}$ represents the quasi-Fermi level for electrons and holes.

$qV_{OC} \rightarrow \Delta\mu_{eh}$ for the conventional solar cell case, which is the case when $T_e = T_h = T_L$. The additional term on the right hand side is the hot carrier term, which increases for larger T_{eh}.

From this expression, one can directly observe how crucial it is to extract carriers at an elevated temperature. A mere increase in quasi-Fermi levels would only lead to a blueshifting of the apparent bandgap, which would actually lead to reduced absorption of a device.

For degenerate systems, only a fraction of the particle population, $\sim k_B T$ around the Fermi level, is involved in cooling the system down. After the initial cooling phase, which lasts 20 ps, the system becomes more and more degenerate as lower-energy states are being filled. Now, only a band of particles with energies $k_B T$ around the Fermi energy is able to contribute to the exchange of energy, as almost all lower-lying states are occupied. The Pauli exclusion principle alters the energy transport properties by limiting the fraction of phase space that is available for electronic transitions.[48] It is the same reason why at lower temperatures, $T \ll T_F$, the electronic heat capacity for a metallic system is on the order of $\sim k_B T$.[45]

Cooling is thus strongly prohibited by band filling, and continues until all energy is fully dissipated away into the phonon bath. By tracking the acceptance rate of scattering events, we see that the acceptance rate drops below 10% at the end of the cooling curves at $\rho = 5 \times 10^{18}$ cm^{-3}, which essentially indicates that cooling occurs on a 10-times longer timescale.

Finally, we turn to the question of whether or not band filling together with the HPB effect can produce ultra-long cooling times. In Figure 6 and Figure 7, a comparison is made between carrier cooling times obtained via hot carrier simulations and via experimentally measured time-resolved photoluminescence (PL) measurements for a $CsSnI_3$ perovskite system.

In our previous work, we have shown that the HPB effect alone is able to extend carrier lifetimes by orders of magnitude.[27] Its origin lies in a mismatch of timescales in the energy cascade. Carriers transfer their energy to LO phonons far more quickly than those phonons can subsequently decay onward. The result is a surplus of LO phonons that drives the reabsorption probability upward. This causes emitted phonons to be recaptured by carriers before their energy can be dissipated as heat, thereby sustaining an elevated carrier temperature. Once the reabsorption

https://doi.org/10.1021/acsenergylett.6c00547
ACS Energy Lett. XXXX, XXX, XXX–XXX

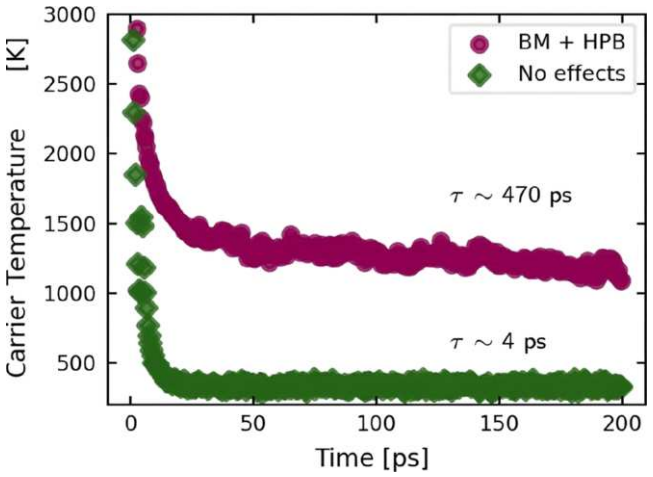

Figure 6. The effect of both band filling and the HPB effect together can extend cooling times to the nanosecond range. Fitting to a simple exponential yields values of $\tau_0 \sim 4$ ps and $\tau_{BM+HPB} \sim 470$ ps at a carrier density of $\rho = 3 \times 10^{18}$ cm^{-3}.

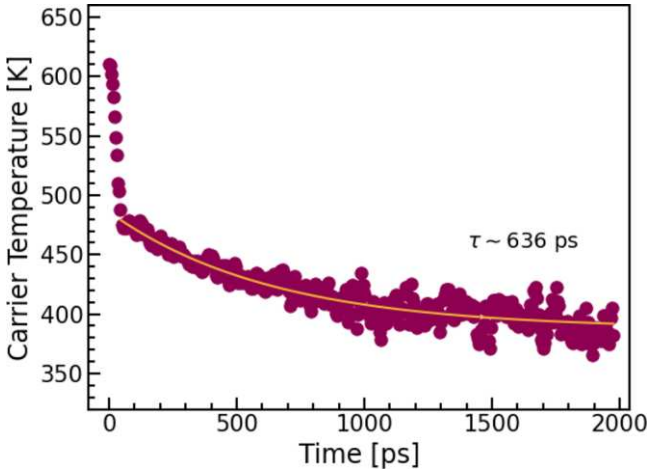

Figure 7. Extracted carrier temperature as a function of time for $CsSnI_3$ at 9×10^{17} cm^{-3} carrier density. Temperatures are obtained by the Boltzmann fitting of the high-energy tail. The slow cooling component is fitted to be around 636 ps.

rate outpaces the LO phonon decay rate at high carrier density, cooling is extended to timescales well in excess of the phonon lifetime. Computationally, we track the evolving LO phonon population after each scattering event and feed the updated occupation back into the LO phonon scattering rates.[27,36]

A strong HPB effect is expected in MHPs, due to a strong overlap between different phonon branches.[18,28] Owing to an ultralow thermal conductivity, further phonon propagation is blocked, increasing the overall upconversion probability.

Figure 6 presents hot carrier simulations for a perovskite-like system, closely related to $CsSnI_3$,[42] with m* = 0.1, $\varepsilon_0 = 26$, $\varepsilon_\infty = 7$, $\omega_0 = 31$ ps^{-1}, at a particle density of $\rho = 3 \times 10^{18}$ cm^{-3}. For the longitudinal optical phonon lifetime, a value of $\tau_{LO} = 0.1$ ps was taken. Both the HPB effect and band filling are active in these simulations and compared with the case where both effects are not active.

The difference in cooling time between the two systems in Figure 6 is remarkable. Fitting both curves from 20 ps onward to a simple exponential, we obtain values of $\tau_0 \sim 4$ ps (no HPB effect and no band filling), and $\tau_{BM+HPB} \sim 470$ ps (both HPB effect and band filling). The interplay of band filling and the HPB effect makes cooling down nearly impossible. As soon as a carrier is allowed to drop down to an empty energy state, an LO phonon is reabsorbed, promoting the carrier to a higher energy state again.

Figure S1 exhibits experimentally measured time-resolved PL traces of $CsSnI_3$ under a pump fluence of 2.2 μJ/cm^2, corresponding to an estimated photogenerated carrier density of 9×10^{17} cm^{-3}.[9] The carrier temperature as a function of time is obtained by fitting their high-energy tail with a Boltzmann equation, accounting for parabolic bands of a 3D bulk semiconductor (see Supporting Information, eq S3). Several fitting procedures were carefully examined to ensure robustness of the result (see Figures S1–S12; Supporting Information section 4).[51−53] The resultant carrier temperature vs time curve is shown in Figure 7. The curves not reaching 300K is likely due to PL Gaussian broadening.[52]

A comparison between Figure 6 and Figure 7 demonstrates that our model is able to reproduce the cooling timescale observed in experimental measurements quite accurately. The simulated cooling time of $\tau_{BM+HPB} \sim 470$ ps corresponds well with the experimental value of $\tau_{exp} \sim 636$ ps. While we do not claim that our model is able to exactly quantify experimental values, we note that the matching of the timescales strongly suggests that no exotic physics, beyond the HPB effect and band filling, is required to quantitatively reach ultra-long carrier cooling times.

Our work should be interpreted as a quantitative minimal model, providing an explicit benchmark for cooling times in MHPs. While many exotic and higher-order effects, such as polaron formation,[13,15,54,55] Auger reheating,[16,56] anharmonicity,[57] spin-orbit coupling,[58,59] all contribute to the carrier cooling dynamics in MHPs, a connection between each phenomenon and an explicit quantitative timescale is often difficult to attribute. This minimal model uncovers that the HPB effect and band filling together can stretch carrier cooling times to the nanosecond range.

Both Figure 6 and Figure 7 exhibit more rapid cooling behavior in their initial cooling phase. In the initial phase, the LO phonon population starts building up by LO phonon emission of carriers cooling down. This activates the HPB effect by bringing the absorption and emission probabilities closer together.[27] Additionally, lower-lying electronic energy states become populated, and prohibit further cooling via band filling. From 30–50 ps onward, carrier cooling is strongly suppressed.

Fitting the high-energy tail of the PL spectrum to a MB distribution does not contradict the earlier statements made about FD vs MB temperature. The high-energy tail of the PL is not affected by the degeneracy of the system and yields the temperature of the distribution indifferent of using a MB or FD fit. The chemical potential only affects the peak of the distribution, not the tail. A translation of the peak energy to an indication for the carrier temperature would be incorrect.

From these results, a significant difference could be expected between different perovskite compositions. In our previous work, the parameter sensitivity of the HPB effect was presented.[27] Together with the parameter sensitivity of band filling depicted above, cooling times could vary by several orders of magnitude for small differences in, for instance, effective mass,

https://doi.org/10.1021/acsenergylett.6c00547
ACS Energy Lett. XXXX, XXX, XXX−XXX

phonon lifetime, or phonon frequency. The combination of both effects is a major factor in explaining the significant differences found in literature.[11] Small differences in effective mass between tin and lead perovskites can translate into large differences in cooling times.

Fundamentally, these findings can be explained by the peculiar material characteristics of MHPs. The polar, but soft, perovskite crystal boosts the HPB effect, while a small effective mass, or narrow electronic density of states, triggers enhanced band filling. This unique combination of material properties creates the opportunity for both the HPB effect and band filling to interact constructively, resulting in the unusual elongation of the hot carrier relaxation time.

An important factor to touch upon is defects. Defects do certainly play a role in hot-carrier dynamics; however, they tend to accelerate cooling rather than elongate it. It has been reported that hot carriers specifically efficiently couple with defects, providing additional cooling pathways through defect states.[28,60] Several reports find more defective perovskites to have a lower hot-carrier PL/TA contribution and faster cooling.[61−64] Lastly, neither higher-energy resonances nor saturation of the trap state is observed in low-temperature carrier density-dependent PL and TA measurements of $FASnI_3$ and $CsSnI_3$.[8,18] We therefore do not attribute the slow cooling observed in Figure 7 to defects.

An LO phonon lifetime τ_{LO} of 0.1 ps was chosen, corresponding with typical values for perovskites.[65] As the phonon lifetime is mostly determined by movement of the A-site cation and the interaction between the two sublattices, we do not expect a lot of difference between lead and tin systems. By using larger values of the phonon lifetime, the role of the A-site cation can be further investigated. Although $CsSnI_3$ has longer phonon dephasing times,[18] larger phonon upconversion coefficients and other higher order anharmonic processes can be captured into a larger resultant phonon lifetime, described by τ_{LO} in our simulations.[27] Doing so would easily extend cooling times to several nanoseconds, corresponding to experimental values obtained by Fang et al. and van de Ven et al.[8,9] for $FASnI_3$ and $MASnI_3$. Unfortunately, these simulations were technically unfeasible due to very long simulation times and instability of the system.

Based on the synergistic interaction between band filling and the hot phonon bottleneck revealed here, we propose the following design roadmap for future hot carrier absorber materials. First, the material must exhibit a low effective mass to minimize the density of states at the band edges; this maximizes the dynamic Burstein–Moss shift and points specifically toward Sn-based compositions over their Pb-based counterparts. Second, a soft phononic lattice characterized by low-frequency optical modes is required to lower the energetic threshold for phonon bottleneck formation. Finally, high material purity is a prerequisite; specifically, the suppression of background doping is critical to prevent the rapid cooling associated with cold-carrier thermalization. It is the simultaneous satisfaction of these electronic, phononic, and chemical criteria, operating under high-injection conditions, that enables the ultra-long cooling times necessary for practical devices.

In this work, the physics behind ultra-long cooling times in metal halide perovskites is presented. It is shown how band filling affects carrier cooling and how carriers affected by band filling remain hot in terms of their Fermi–Dirac temperature for extended periods of time. A combination of band filling with the HPB effect is able to produce ultra-long cooling times for a tin perovskite system, indicating the strong potential for future hot carrier solar cell applications.

Crucially, our simulations confirm that the 'hot' carriers maintained by this synergistic mechanism retain a high thermodynamic Fermi–Dirac temperature ($T_{e/h}$), rather than merely possessing high average kinetic energy due to degenerate state filling. This distinction is vital for photovoltaic applications. As described by the fundamental hot carrier solar cell equation, the potential open-circuit voltage boost is directly proportional to the Carnot efficiency term $(1 - T_L/T_{e/h})$. By demonstrating that $T_{e/h}$ remains significantly elevated (>600 K) on nanosecond timescales, we confirm that Sn-based perovskites can theoretically access this thermodynamic voltage enhancement. Consequently, the ultralong cooling times reported here represent a viable pathway to exceeding the Shockley–Queisser limit, identifying low-effective-mass Sn-perovskites as a priority material for next-generation hot carrier devices.

■ ASSOCIATED CONTENT

Supporting Information

The Supporting Information is available free of charge at https://pubs.acs.org/doi/10.1021/acsenergylett.6c00547.

Sample preparation, TRPL Spectroscopy, and sensitivity of fitting procedure (PDF)

■ AUTHOR INFORMATION

Corresponding Author

L. Jan Anton Koster – *Zernike Institute for Advanced Materials, University of Groningen, Nijenborgh 3, Groningen, AG 9747, The Netherlands;* orcid.org/0000-0002-6558-5295; Email: l.j.a.koster@rug.nl

Authors

Tim Faber – *Zernike Institute for Advanced Materials, University of Groningen, Nijenborgh 3, Groningen, AG 9747, The Netherlands*

Larissa J. M. van de Ven – *Zernike Institute for Advanced Materials, University of Groningen, Nijenborgh 3, Groningen, AG 9747, The Netherlands; LMPV-Sustainable Energy Materials Department, University of Groningen, AMOLF, Amsterdam, 1098 XG, Netherlands*

Lado Filipovic – *CDL for Multi-Scale Process Modeling of Semiconductor Devices and Sensors at the Institute for Microelectronics, TU Wien, Gusshausstrasse 27-29, 1040 Vienna , Austria;* orcid.org/0000-0003-1687-5058

Maria Antonietta Loi – *Zernike Institute for Advanced Materials, University of Groningen, Nijenborgh 3, Groningen, AG 9747, The Netherlands;* orcid.org/0000-0002-7985-7431

Complete contact information is available at: https://pubs.acs.org/doi/10.1021/acsenergylett.6c00547

Notes

The authors declare no competing financial interest.

■ ACKNOWLEDGMENTS

The authors would like to thank the Center for Information Technology of the University of Groningen for their support and for providing access to the Peregrine high-performance computing cluster, the Zernike Institute for Advanced

Materials for funding. The financial support by the Austrian Federal Ministry of Labour and Economy and the National Foundation for Research, Technology and Development and the Christian Doppler Research Association is gratefully acknowledged. Financial support by the Austrian Science Fund (FWF) through projects [10.55776/DOC142 and 10.55776/P35318].

■ REFERENCES

(1) Shockley, W.; Queisser, H. J. Detailed balance limit of efficiency of p-n junction solar cells. *J. Appl. Phys.* **1961**, *32*, 510–519.
(2) Ross, R. T.; Nozik, A. J. Efficiency of hot-carrier solar energy converters. *J. Appl. Phys.* **1982**, *53*, 3813–3818.
(3) König, D.; Casalenuovo, K.; Takeda, Y.; Conibeer, G.; Guillemoles, J. F.; Patterson, R.; Huang, L. M.; Green, M. A. Hot carrier solar cells: Principles, materials and design. *Phys. E* **2010**, *42*, 2862–2866.
(4) Le Bris, A.; Guillemoles, J. F. Hot carrier solar cells: Achiev-able efficiency accounting for heat losses in the absorber and through contacts. *Appl. Phys. Lett.* **2010**, *97*, No. 113506.
(5) Kahmann, S.; Loi, M. A. Hot carrier solar cells and the potential of perovskites for breaking the Shockley-Queisser limit. *J. Mater. Chem. C* **2019**, *7*, 2471.
(6) Takeda, Y.; Motohiro, T.; König, D.; Aliberti, P.; Feng, Y.; Shrestha, S.; Conibeer, G. Practical factors lowering conver-sion efficiency of hot carrier solar cells. *Appl. Phys. Express* **2010**, *3*, No.104301.
(7) Nelson, J., *The Physics Of Solar Cells*; World Scientific Publishing Company: Singapore, **2003**.
(8) Fang, H. H.; Adjokatse, S.; Shao, S.; Even, J.; Loi, M. A. Long-lived hot-carrier light emission and large blue shift in formami-dinium tin triiodide perovskites. *Nat. Commun.* **2018**, *9*, No. 243.
(9) van de Ven, L. J. M.; Tekelenburg, E. K.; Pitaro, M.; Pinna, J.; Loi, M. A. Cation influence on hot-carrier relaxation in tin triiodide perovskite thin films. *ACS Energy Lett.* **2024**, *9*, 992.
(10) Li, M.; Fu, J.; Xu, Q.; Sum, T. C. Slow hot-carrier cooling in halide perovskites: Prospects for hot-carrier solar cells. *Adv. Mater.* **2019**, *31*, No.1802486.
(11) Fu, J.; Ramesh, S.; Melvin Lim, J. W.; Sum, T. C. Carriers, quasiparticles, and collective excitations in halide perovskites. *Chem. Rev.* **2023**, *123*, 8154.
(12) Faber, T.; Filipovic, L.; Koster, L. J. The role of thermalization in the cooling dynamics of hot carrier solar cells. *Sol. RRL* **2023**, *7*, No. 2300140.
(13) Zhu, H.; Miyata, K.; Fu, Y.; Wang, J.; Joshi, P. P.; Niesner, D.; Williams, K. W.; Jin, S.; Zhu, X. Y. Screening in crystalline liquids pro-tects energetic carriers in hybrid perovskites. *Science* **2016**, *353*, 1409.
(14) Niesner, D.; Zhu, H.; Miyata, K.; Joshi, P. P.; Evans, T. J. S.; Kudisch, B. J.; Trinh, M. T.; Marks, M.; Zhu, X. Y. Persistent energetic electrons in methylammonium lead iodide perovskite thin films. *J. Am. Chem. Soc.* **2016**, *138*, 15717.
(15) Frost, J. M.; Whalley, L. D.; Walsh, A. Slow cooling of hot polarons in halide perovskite solar cells. *ACS Energy Lett.* **2017**, *2*, 2647–2652.
(16) Fu, J.; Xu, Q.; Han, G.; Wu, B.; Huan, C. H. A.; Leek, M. L.; Sum, T. C. Hot carrier cooling mechanisms in halide perovskites. *Nat. Commun.* **2017**, *8*, No.1300.
(17) Papagiorgis, P.; Protesescu, L.; Kovalenko, M. V.; Othonos, A.; Itskos, G. Long-lived hot carriers in formamidinium lead iodide nanocrystals. *J. Phys. Chem. C* **2017**, *121*, 12434.
(18) Tekelenburg, E. K.; Camargo, F. V. A.; Filippetti, A.; Mattoni, A.; van de Ven, L. J. M.; Pitaro, M.; Cerullo, G.; Loi, M. A. Mechanism of hot-carrier photoluminescence in Sn-based perovskites. *Adv. Mater.* **2025**, *37*, No. 2411892.
(19) Yin, J.; Maity, P.; Naphade, R.; Cheng, B.; He, J. H.; Bakr, O. M.; Brédas, J. L.; Mohammed, O. F. Tuning hot carrier cooling dy-namics by dielectric confinement in two-dimensional hybrid perovskite crystals. *ACS Nano* **2019**, *13*, 12621.
(20) Li, M.; Begum, R.; Fu, J.; Xu, Q.; Koh, T. M.; Veldhuis, S. A.; Grätzel, M.; Mathews, N.; Mhaisalkar, S.; Sum, T. C. Low threshold and efficient multiple exciton generation in halide perovskite nanocrystals. *Nat. Commun.* **2018**, *9*, No. 4197.
(21) Dai, L.; Deng, Z.; Auras, F.; Goodwin, H.; Zhang, Z.; Walmsley, J. C.; Bristowe, P. D.; Deschler, F.; Greenham, N. C. Slow carrier relaxation in tin-based perovskite nanocrystals. *Nat. Photonics* **2021**, *15*, 696.
(22) Burstein, E. Anomalous optical absorption limit in InSb. *Phys. Rev.* **1954**, *93*, No. 632.
(23) Moss, T. S. The interpretation of the properties of indium antimonide. *Proc. Phys. Soc., London, Sect. B* **1954**, *67*, 775.
(24) Wright, A. D.; Verdi, C.; Milot, R. L.; Eperon, G. E.; Pérez-Osorio, M. A.; Snaith, H. J.; Giustino, F.; Johnston, M. B.; Herz, L. M. Electron–phonon coupling in hybrid lead halide perovskites. *Nat. Commun.* **2016**, *7*, No. 11755.
(25) Manser, J. S.; Kamat, P. V. Band filling with free charge carriers in organometal halide perovskites. *Nat. Photonics* **2014**, *8*, 737.
(26) Filippetti, A.; Kahmann, S.; Caddeo, C.; Mattoni, A.; Saba, M.; Bosin, A.; Loi, M. A. Fundamentals of tin iodide perovskites: A promising route to highly efficient, lead-free solar cells. *J. Mater. Chem. A* **2021**, *9*, 11812.
(27) Faber, T.; Filipovic, L.; Koster, L. J. The hot phonon bottleneck effect in metal halide perovskites. *J. Phys. Chem. Lett.* **2024**, *15*, 12601.
(28) Yang, J.; Wen, X.; Xia, H.; Sheng, R.; Ma, Q.; Kim, J.; Tapping, P.; Harada, T.; Kee, T. W.; Huang, F.; et al. Acoustic-optical phonon upconversion and hot-phonon bottleneck in lead-halide perovskites. *Nat. Commun.* **2017**, *8*, No. 14120.
(29) Price, M. B.; Butkus, J.; Jellicoe, T. C.; Sadhanala, A.; Briane, A.; Halpert, J. E.; Broch, K.; Hodgkiss, J. M.; Friend, R. H.; Deschler, F. Hot carrier cooling and photoinduced refractive index changes in organic-inorganic lead halide perovskites. *Nat. Commun.* **2015**, *6*, 8420.
(30) Sekiguchi, F.; Hirori, H.; Yumoto, G.; Shimazaki, A.; Nakamura, T.; Wakamiya, A.; Kanemitsu, Y. Enhancing the hot-phonon bottleneck effect in a metal halide perovskite by terahertz phonon excitation. *Phys. Rev. Lett.* **2021**, *126*, No. 077401.
(31) Yang, Y.; Ostrowski, D. P.; France, R. M.; Zhu, K.; van de Lagemaat, J.; Luther, J. M.; Beard, M. C. Observation of a hot-phonon bottleneck in lead-iodide perovskites. *Nat. Photonics* **2016**, *10*, 53.
(32) Jacoboni, C.; Lugli, P. *The Monte Carlo Method for Semi-conductor Device Simulation*; Computational Microelectronics. Springer Vienna: USA, **2011**.
(33) Jacoboni, C.; Reggiani, L. The Monte Carlo method for the solution of charge transport in semiconductors with applications to covalent materials. *Rev. Mod. Phys.* **1983**, *55*, No. 645.
(34) Tomizawa, K. *Numerical Simulation of Submicron Semiconductor Devices*; Artech House Publishers: USA, **1993**.
(35) Hockney, R.; Eastwood, J. *Computer Simulation Using Particles*; CRC Press: USA, **1988**.
(36) Ferry, D. K., *In Hot Carriers in Semiconductors, 2053-2563, 7–1 to 7–49*. IOP Publishing: USA, **2021**.
(37) Kosina, H.; Nedjalkov, M.; Selberherr, S. Theory of the Monte Carlo method for semiconductor device simulation. *IEEE Trans. Electron Devices* **2000**, *47*,1898–1908.
(38) Poncé, S.; Schlipf, M.; Giustino, F. Origin of low carrier mobilities in halide perovskites. *ACS Energy Lett.* **2019**, *4*, No. 456.
(39) Schlipf, M.; Poncé, S.; Giustino, F. Carrier lifetimes and polaronic mass enhancement in the hybrid halide perovskite $CH3NH3PbI_3$ from multiphonon Fröhlich coupling. *Phys. Rev. Lett.* **2018**, *121*, No. 086402.
(40) Hellwarth, R. W.; Biaggio, I. Mobility of an electron in a multimode polar lattice. *Phys. Rev. B* **1999**, *60*, No. 299.
(41) Lan, Y.; Dringoli, B. J.; Valverde-Chávez, D. A.; Ponseca, C. S.; Sutton, M.; He, Y.; Kanatzidis, M. G.; Cooke, D. G. Ultrafast correlated charge and lattice motion in a hybrid metal halide perovskite. *Sci. Adv.* **2019**, *5*, No. eaaw5558.

(42) Frost, J. M. Calculating polaron mobility in halide perovskites. *Phys. Rev. B* **2017**, *96*, No. 195202.
(43) Irvine, L. A.; Walker, A. B.; Wolf, M. J. Quantifying polaronic effects on the scattering and mobility of charge carriers in lead halide perovskites. *Phys. Rev. B* **2021**, *103*, No. L220305.
(44) Muñoz, M.; Pollak, F. H.; Kahn, M.; Ritter, D.; Kronik, L.; Cohen, G. M. Burstein-Moss shift of n-doped $In_{0.53}Ga_{0.47}As/InP$. *Phys. Rev. B* **2001**, *63*, No. 233302.
(45) Ashcroft, N. W.; Mermin, N. D. *Solid State Physics, college edn.* **1976**.
(46) Umari, P.; Mosconi, E.; De Angelis, F. Relativistic GW calculations on $CH_3NH_3PbI_3$ and $CH_3NH_3SnI_3$ perovskites for solar cell applications. *Sci. Rep.* **2014**, *4*, No. 4467.
(47) Richter, J. M.; Branchi, F.; Valduga de Almeida Camargo, F.; Zhao, B.; Friend, R. H.; Cerullo, G.; Deschler, F. Ultrafast car-rier thermalization in lead iodide perovskite probed with two-dimensional electronic spectroscopy. *Nat. Commun.* **2017**, *8*, No. 376.
(48) Lugli, P.; Ferry, D. K. Degeneracy in the ensemble Monte Carlo method for high-field transport in semiconductors. *IEEE Trans. Electron Devices* **1985**, *32*, 2431.
(49) Zebarjadi, M.; Bulutay, C.; Esfarjani, K.; Shakouri, A. Monte Carlo simulation of electron transport in degenerate and inhomogeneous semiconductors. *Appl. Phys. Lett.* **2007**, *90*, No. 092111.
(50) Würfel, P.; Würfel, U. *Physics of Solar Cells: From Basic Principles to Advanced Concepts*; John Wiley & Sons: **2016**.
(51) Tanghe, I.; Lin, C. Y.; Wagner, I.; Samoli, M.; Ataberk Cayan, S.; Hens, Z.; Hodgkiss, J.; Chen, K.; Geiregat, P. Determination of the car-rier temperature in weakly confined semiconductor nanocrystals using time-resolved optical spectroscopy. *Nanoscale* **2025**, *17*, 4381.
(52) Savill, K. J.; Klug, M. T.; Milot, R. L.; Snaith, H. J.; Herz, L. M. Charge-carrier cooling and polarization memory loss in formamidinium tin triiodide. *J. Phys. Chem. Lett.* **2019**, *10*, No. 6038.
(53) Lim, J. W. M.; Giovanni, D.; Righetto, M.; Feng, M.; Mhaisalkar, S. G.; Mathews, N.; Sum, T. C. Hot carriers in halide perovskites: how hot truly? *J. Phys. Chem. Lett.* **2020**, *11*, 2743.
(54) Evans, T. J. S.; Miyata, K.; Joshi, P. P.; Maehrlein, S.; Liu, F.; Zhu, X. Y. Competition between hot-electron cooling and large polaron screening in $CsPbBr_3$ perovskite single crystals. *J. Phys. Chem. C* **2018**, *122*, 13724.
(55) Joshi, P. P.; Maehrlein, S. F.; Zhu, X. Dynamic screening and slow cooling of hot carriers in lead halide perovskites. *Adv. Mater.* **2019**, *31*, No. 1803054.
(56) Shen, J.; Zhang, X.; Das, S.; Kioupakis, E.; Van de Walle, C. G. Unexpectedly strong Auger recombination in halide perovskites. *Adv. Energy Mater.* **2018**, *8*, No. 1801027.
(57) Li, W.; Vasenko, A. S.; Tang, J.; Prezhdo, O. V. Anharmonicity extends carrier lifetimes in lead halide perovskites at elevated temperatures. *J. Phys. Chem. Lett.* **2019**, *10*, 6219.
(58) Kepenekian, M.; Robles, R.; Katan, C.; Sapori, D.; Pedesseau, L.; Even, J. Rashba and Dresselhaus effects in hybrid organic–inorganic perovskites: From basics to devices. *ACS Nano* **2015**, *9*, 11557.
(59) Zheng, F.; Tan, L. Z.; Liu, S.; Rappe, A. M. Rashba spin–orbit coupling enhanced carrier lifetime in $CH_3NH_3PbI_3$. *Nano Lett.* **2015**, *15*, 7794.
(60) Righetto, M.; Lim, S. S.; Giovanni, D.; Lim, J. W. M.; Zhang, Q.; Ramesh, S.; Tay, Y. K. E.; Sum, T. C. Hot carriers perspective on the nature of traps in perovskites. *Nat. Commun.* **2020**, *11*, No. 2712.
(61) Dai, L.; Ye, J.; Greenham, N. C. Thermalization and relaxation mediated by phonon management in tin-lead perovskites. *Light: Sci. Appl.* **2023**, *12*, No. 208.
(62) Kahmann, S.; Shao, S.; Loi, M. A. Cooling, scattering, and recombination—the role of the material quality for the physics of tin halide perovskites. *Adv. Funct. Mater.* **2019**, *29*, No. 1902963.
(63) Jiang, X.; Hoffman, J.; Stoumpos, C. C.; Kanatzidis, M. G.; Harel, E. Transient sub-band-gap states at grain boundaries of $CH_3NH_3PbI_3$ perovskite act as fast temperature relaxation cen-ters. *ACS Energy Lett.* **2019**, *4*, 1741.
(64) Wang, T.; Jin, L.; Hidalgo, J.; Chu, W.; Snaider, J. M.; Deng, S.; Zhu, T.; Lai, B.; Prezhdo, O.; Correa-Baena, J. P.; Huang, L.; et al. Protecting hot carriers by tuning hybrid perovskite structures with alkali cations. *Sci. Adv.* **2020**, *6*, No. eabb1336.
(65) Leguy, A. M.; Goñi, A. R.; Frost, J. M.; Skelton, J.; Brivio, F.; Rodríguez-Martínez, X.; Weber, O. I.; Pallipurath, A.; Alonso, M. I.; Campoy-Quiles, M.; et al. Dynamic disorder, phonon lifetimes, and the assignment of modes to the vibrational spectra of methylammonium lead halide perovskites. *Phys. Chem. Chem. Phys.* **2016**, *18*, 27051.

https://doi.org/10.1021/acsenergylett.6c00547
ACS Energy Lett. XXXX, XXX, XXX–XXX